UKAEA FUS 428

EURATOM/UKAEA Fusion

Numerical simulations of tokamak plasma turbulence and internal transport barriers

A Thyagaraja

May 2000

EURATOM/UKAEA Fusion Association

Culham Science Centre, Abingdon
Oxfordshire, OX14 3DB
United Kingdom
Telephone +44 1235 463449
Facsimile +44 1235 463647

Numerical simulations of tokamak plasma turbulence and internal transport barriers

A. Thyagaraja

EURATOM/UKAEA Fusion Association, Culham Science Centre, Abingdon, OX14 3DB, UK.

Abstract

A wide variety of magnetically confined plasmas, including many tokamaks such as JET, TFTR, JT-60U, DIII-D, RTP show clear evidence for the existence of the so-called 'internal transport barriers' (ITBs) which are regions of relatively good confinement, associated with substantial gradients in temperature and/or density. A computational approach to investigating the properties of tokamak plasma turbulence and transport is developed. This approach is based on the evolution of global, two-fluid, nonlinear, electromagnetic plasma equations of motion with specified sources. In this paper, the computational model is applied to the problem of determining the nature and physical characteristics of barrier phenomena, with particular reference to RTP (electron-cyclotron resonance heated) and JET (neutral beam heated) observations of ITBs. The simulations capture features associated with the formation of these internal transport barriers, and qualitatively reproduce some of the observations made on RTP and JET. The picture of plasma turbulence suggested involves variations of temperature and density profiles induced by the electromagnetic fluctuations, on length scales intermediate between the system size and the ion Larmor radius, and time scales intermediate between the confinement time and the Alfvén time (collectively termed, 'mesoscales'). The back-reaction of such profile 'corrugations' (features exhibiting relatively high local spatial gradients and rapid time variations) on the development and saturation of the turbulence itself plays a key role in the nonlinear dynamics of the system. The corrugations are found to modify the dynamical evolution of radial electric field shear and the bootstrap current density, which in turn influence the turbulence. The interaction is mediated by relatively long wavelength, electromagnetic modes excited by an inverse cascade and involving nonlinear instabilities and relaxation phenomena such as intermittency and internal mode locking.

I. Introduction

Recent experimental researches on anomalous transport in tokamaks [1, 2, 3, 4, 5] have revealed a wealth of fascinating phenomena associated with the spontaneous formation of the so-called *internal transport barriers* (ITBs). For instance, in the RTP tokamak[1], keeping the total current, line-averaged density and heating power fixed, when the electron cyclotron heating (ECH) power deposition radius, r_{dep}, was varied across the minor cross section, the steady state central electron temperature exhibited discrete 'jumps' (Fig.2 in [1]), which were correlated with the passage of the narrow power deposition profile across surfaces where the safety factor q had low order rational values. Moreover, the electron temperature profiles measured using high precision Thomson scattering diagnostics showed considerable 'fine structure' and other features, reproduced in Fig.1(Fig.3a, *loc.cit.* and also Fig.4 of this paper). These observations were phenomenologically[1] explained by assuming that the effective electron perpendicular thermal diffusivity, χ_e, has strong, narrow minima at rational values of q. In addition, an outward 'thermal advection' was invoked to account for the apparent lowering of central electron temperature below the Ohmic value during off-axis heating. These results present a challenge to *any* first principles theory of plasma transport. It should be stressed that in larger tokamaks, with ion heating (for an excellent recent discussion with comprehensive references, see [4]), the conditions are somewhat different, and other mechanisms may be operative. A complete theoretical understanding of ITBs in general, and RTP observations in particular, does not exist, although several suggestions [6, 7, 8] have been put forward as to the possible causes.

Anomalous transport in tokamaks is believed to be due to plasma turbulence. The most important physical manifestations of this turbulence occur at frequencies of the order of the 'drift frequency', $\omega_* \simeq (C_s/L_n)(k_\perp \rho_s)$ ($\omega_* \ll \omega_{ci} = eB_0/m_i c$), although larger than the inverse energy confinement time, $1/\tau_E$ (where, $\rho_s = C_s/\omega_{ci}; C_s^2 = (T_i + T_e)/m_i$, and L_n is a typical density scale length of the equilibrium density profile). Furthermore, the wavelengths of typical tokamak turbulent fluctuations are characteristic of drift modes, and are somewhat longer than the ion gyroradius (thus one finds experimentally that $k_\perp \rho_s \simeq 0.1$). This intermediate regime is conveniently termed[10] the 'mesoscale'. A possible approach to tokamak turbulence and transport involves the global (ie, 'whole tokamak') solution of the two-fluid plasma and Maxwell's equations in this regime of interest. The tool employed to implement this approach is a global, electromagnetic, quasi-neutral, two-fluid code CUTIE[9, 10]. The simulations described in this paper present a picture of mesoscale dynamics which involves nonlinear interactions between the plasma profiles (eg. those of $n_e, T_{e,i}$ etc) and the electromagnetic turbulence. These interactions are critically influenced by turbulent advection of the density, temperature and current, and its ability to 'corrugate' their profiles. Such relatively rapid spatio-temporal variations have dual effects on the turbulence involving the sheared radial electric fields (an example from JT-60U given by Gormezano (1999)[2], is shown in Fig.3) and bootstrap currents generated by the corrugated profiles. On the one hand,

gradients in pressure, density and current density can destabilize various linear and nonlinear instabilities. Interestingly, they also have strongly *stabilizing* effects due to sheared radial electric fields[8] (associated with p', n'; here and elsewhere, primes on equilibrium quantities indicate radial derivatives), and magnetic fields[7] (associated with q', j'). This complex interplay between profiles and turbulent fluctuations in electromagnetic fields involves both 'inverse cascades' (energy transfer from short to long wavelengths) [11], and 'direct cascades' due to secondary, short wavelength/high frequency instabilities driven by long wavelength modes leading to intermittency and current filamentation (observed for example, in the RTP experiments[12]; see Fig.4). It is of interest to note that in a recent paper, Zeiler *et al*[13] identify the crucial role of nonlinearity, electromagnetic effects, nonadiabaticity and the resultant profile-turbulence interactions in η_i turbulence at the tokamak edge.

In this paper, CUTIE simulations of the RTP experiments[1](an electron-heated tokamak), and recent computations of ITB formation for typical JET-like conditions [2] (involving NBI and strong plasma toroidal rotation induced by the beams) are presented. Results obtained thus far are encouraging and suggest that essential qualitative features of the observations made in real experiments are indeed captured by the model. The paper is organized as follows: in Section II, the physical basis of CUTIE, the governing equations of motion used, and the computational method are described. Readers interested in results can skim this section for an overview and notation and proceed to the next one directly. Section III presents the results obtained in both RTP and JET simulations and a comparison with experiment. Section IV provides a brief discussion and conclusions.

II. Physics basis of CUTIE and computational approach

CUTIE is based on a periodic cylinder model ($r, \theta, \zeta \equiv z/R$) of the tokamak, with equilibrium flux surfaces assumed to be concentric circles[9, 10]. The Shafranov shift and metric variations neglected at present are relatively unimportant for RTP, which has nearly circular flux surfaces, although not in JET, which has significant 'shaping' of the flux surfaces. These effects will be investigated in future work. However, field-line curvature and line-bending are crucial[14, 15] for the dynamics, and are taken into account in the equations of motion for the turbulent fluctuations. All plasma properties (e.g the electron density, n_e) are written as a sum of a flux-surface averaged 'mean', $n_0(r,t)$, and a 'fluctuation', $\delta n_e(r,\theta,\zeta,t)$. Thus we write, $n_e(r,\theta,\zeta,t) \equiv n_0(r,t) + \delta n_e$, where, $n_0(r,t) \equiv < n_e > = \int_0^{2\pi}\int_0^{2\pi} n_e(r,\theta,\zeta,t)\frac{d\theta d\zeta}{4\pi^2}$, and $\delta n_e/N^* \equiv n^*(r,\theta,\zeta,t)$, where $N^* = n_0(0,t)$. Note that N^* is a 'representative' density (taken to be $n_0(0,t)$). This decomposition is not a 'linearization', although in practice, the relative fluctuations are small. Nondimensional fluctuations such as n^* are represented by the Fourier expansion:

$$n^* = \sum_{m=-\infty}^{\infty}\sum_{n=-\infty}^{\infty} \hat{n}_{m,n}(r,t)\exp(im\theta + in\zeta) \qquad (1)$$

By definition, the 'mean' $n_0(r,t)$ represents the $m = n = 0$ Fourier component of the density, and consequently, $\hat{n}_{0,0} \equiv 0$. Since all plasma fields considered are real, the Fourier coefficients satisfy the reality condition, $\hat{n}_{m,n} = \bar{\hat{n}}_{-m,-n}$, where the over-bar denotes complex conjugation.

The essential physics approximations used are: quasi-neutrality, $\nabla.\mathbf{j} = 0$; reduced tokamak ordering (ie, fast magnetosonic waves are eliminated and $\delta B_{||}$ fluctuations are neglected); neglect of electron inertia and trapped particle dynamics, apart from the use of neoclassical transport coefficients[14], including the bootstrap current. The electromagnetic fields are described in terms of two potentials, ϕ and ψ. These are *fluctuating* parts(thus, $\delta\mathbf{E} = -\nabla\phi - \frac{1}{c}\frac{\partial\psi}{\partial t}\mathbf{e}_\zeta$). The corresponding 'mean' quantities are denoted by, $\Phi_0(r,t), \Psi_0(r,t)$. This two-fluid system is described by the four variables, n_e, T_e, T_i, and $v_{||i}$, which satisfy the four conservation equations representing electron continuity, electron and ion energy balance and the ion parallel momentum balance, respectively. The two potentials are evolved using the quasi-neutrality condition and the generalized Ohm's law. In practice the electron temperature fluctuations are small compared to the density fluctuations, due to the large parallel thermal diffusivity (of order qRv_{th}).

The following dimensional parameters are used: $\bar{V}_A^2 = B_0^2/4\pi m_i n(0,t); \bar{V}_{th}^2 = (T_e(0,t) + T_i(0,t))/m_i; \omega_{ci} = eB_0/m_i c; \rho_s = \bar{V}_{th}/\omega_{ci}; \beta = (\bar{V}_{th}/\bar{V}_A)^2$. In addition, we introduce the 'potential vorticity' (with dimensions, [1/T]), $\Theta = \nabla.(\frac{n_0(r,t)}{n_0(0,t)}\nabla_\perp\frac{c\phi}{B_0})$. We define the nondimensional fluctuating quantities, $\phi^*, \psi^*, \Theta^*, n^*, \xi^*, \lambda_{i,e}^* : \frac{c\phi}{B_0} = \bar{V}_{th}\rho_s\phi^*; \frac{\psi}{B_0} = \rho_s\beta^{1/2}\psi^*$ $\Theta = \frac{\bar{V}_{th}}{\rho_s}\Theta^*; \Theta^* = \rho_s^2\nabla.(\frac{n_0(r,t)}{N^*}\nabla_\perp\phi^*)$; $n^* = \delta n_e/N^*; \lambda_{i,e}^* = \delta T_{i,e}/T^*; \xi^* = n_0(r,t)\delta v_{||}/\bar{\xi}$, where, $N^* = n_e(0,t), T^* = T_e(0,t) + T_i(0,t)$, and $\bar{\xi} = N^*\bar{V}_{th}$. The system is thus described by these variables and the corresponding 'mean' quantities, which are conveniently chosen to be, $n_0(r,t), T_{e0}(r,t), T_{i0}(r,t), v_{\theta 0}(r,t), v_{\zeta 0}(r,t), E_{r0}(r,t), B_{\theta 0}(r,t)$.

The derivations of the evolution equations from first principles is well-known[14],[15]). Several different advection velocities[14, 17] occur in the theory. By definition, $E_{r0} = -\frac{\partial\Phi_0}{\partial r}$. The velocity, $\mathbf{u}_0 = -\frac{cE_{r0}}{B}\mathbf{e}_\theta + \mathbf{b}_0 v_{||0}$ represents the equilibrium 'MHD' flow of the plasma (ions), whilst $\mathbf{u}_{e0}$ represents the corresponding electron flow, $\mathbf{u}_{e0} = -\frac{cE_{r0}}{B}\mathbf{e}_\theta + \mathbf{b}_0(v_{||0} - j_{||0}/en_0)$. The ion fluid flow (ie, MHD flow + diamagnetic flow) is given by, $\mathbf{v}_0 = \mathbf{u}_0 + \frac{c}{en_0B}\frac{\partial p_{i0}}{\partial r}\mathbf{e}_\theta$. We also have the relation, $\Theta_0 = \frac{1}{r}\frac{\partial}{\partial r}(\frac{rn_0(r,t)}{N^*}\frac{c}{B_0}\frac{\partial\Phi_0}{\partial r})$. Finally, $\mathbf{v}_{e0} = -\left[\frac{cE_{r0}}{B} + \frac{c}{en_0B}\frac{\partial p_{e0}}{\partial r}\right]\mathbf{e}_\theta$ is the total electron *poloidal flow* composed of the electron $\mathbf{E}\times\mathbf{B}$ equilibrium flow and the electron diamagnetic flow. In the following, $\nabla_{||} \equiv \mathbf{b}_0.\nabla = \frac{1}{qR}(\frac{\partial}{\partial\theta} + q\frac{\partial}{\partial\zeta})$, (ie, the gradient in the direction of the *unperturbed field*). The nonlinear terms account for the exact field direction. The equations of motion for the fluctuations, including the definition of Θ^*, are the following:

$$\Theta^* = \rho_s^2\nabla.(\frac{n_0}{N^*}\nabla_\perp\phi^*) \tag{2}$$

$$\frac{\partial \Theta^*}{\partial t} + \mathbf{v}_0.\nabla\Theta^* + \bar{V}_A\nabla_\parallel\rho_s^2\nabla_\perp^2\psi^* = \bar{V}_A\rho_s\frac{1}{r}\frac{\partial\psi^*}{\partial\theta}\frac{4\pi\rho_s}{cB_0}j_0' + \bar{V}_{th}\rho_s\frac{1}{r}\frac{\partial(\psi^*,\rho_s^2\nabla_\perp^2\psi^*)}{\partial(r,\theta)}$$
$$+\bar{V}_{th}\rho_s\left[\frac{1}{r}\frac{\partial(\Theta^*,\phi^*)}{\partial(r,\theta)} + (\frac{N^*T_{i0}}{n_0T^*})\frac{1}{r}\frac{\partial(\Theta^*,n^*)}{\partial(r,\theta)}\right]$$
$$-\frac{2\bar{V}_{th}\rho_s}{R_0}\left[\frac{\cos\theta}{r}\frac{\partial p^*}{\partial\theta} + \sin\theta\frac{\partial p^*}{\partial r}\right] + \rho_s^2\Theta_0'\frac{1}{r}\frac{\partial\phi^*}{\partial\theta}$$
$$+\Sigma_\Theta^* \tag{3}$$

$$\frac{\partial\psi^*}{\partial t} + \mathbf{v}_{e0}.\nabla\psi^* + \bar{V}_A\nabla_\parallel\phi^* = \bar{V}_A(\frac{N^*T_{e0}}{n_0T^*})\nabla_\parallel n^*$$
$$+\bar{V}_{th}\rho_s\left[\frac{1}{r}\frac{\partial(\psi^*,\phi^*)}{\partial(r,\theta)} - (\frac{N^*T_{e0}}{n_0T^*})\frac{1}{r}\frac{\partial(\psi^*,n^*)}{\partial(r,\theta)}\right] + \Sigma_\psi^* \tag{4}$$

$$\frac{\partial n^*}{\partial t} + \mathbf{u}_{e0}.\nabla n^* + \bar{V}_A\nabla_\parallel\rho_s^2\nabla_\perp^2\psi^* = \bar{V}_A\rho_s\frac{1}{r}\frac{\partial\psi^*}{\partial\theta}\frac{4\pi\rho_s}{cB_0}j_0' + \bar{V}_{th}\rho_s\frac{1}{r}\frac{\partial(\psi^*,\rho_s^2\nabla_\perp^2\psi^*)}{\partial(r,\theta)}$$
$$+\bar{V}_{th}\rho_s\frac{1}{r}\frac{\partial(n^*,\phi^*)}{\partial(r,\theta)} + \bar{V}_{th}\rho_s(\frac{n_0'}{N^*})\frac{1}{r}\frac{\partial\phi^*}{\partial\theta}$$
$$-\frac{2\bar{V}_{th}\rho_s}{R_0}\left[\frac{\cos\theta}{r}\frac{\partial p_e^*}{\partial\theta} + \sin\theta\frac{\partial p_e^*}{\partial r}\right]$$
$$-\bar{V}_{th}\nabla_\parallel\xi^* + \Sigma_n^* \tag{5}$$

$$\frac{\partial\xi^*}{\partial t} + \mathbf{u}_0.\nabla\xi^* + \bar{V}_{th}(\frac{T_{e0}+T_{i0}}{T^*})\nabla_\parallel n^* = (\frac{n_0v_{\parallel 0}'}{N^*})\rho_s\frac{1}{r}\frac{\partial\phi^*}{\partial\theta} + \bar{V}_{th}\rho_s\frac{1}{r}\frac{\partial(\xi^*,\phi^*)}{\partial(r,\theta)}$$
$$-\bar{V}_{th}\rho_s\beta^{1/2}(\frac{p_0'}{P^*})\frac{1}{r}\frac{\partial\psi^*}{\partial\theta} - \bar{V}_{th}\rho_s\beta^{1/2}\frac{1}{r}\frac{\partial(p^*,\psi^*)}{\partial(r,\theta)}$$
$$-\bar{V}_{th}(\frac{n_0}{N^*})\nabla_\parallel(\lambda_i^* + \lambda_e^*) + \Sigma_\xi^* \tag{6}$$

$$\frac{3}{2}\left[\frac{\partial\lambda_i^*}{\partial t} + \mathbf{u}_0.\nabla\lambda_i^*\right] + \bar{V}_{th}(\frac{N^*T_{i0}}{n_0T^*})\nabla_\parallel\xi^* = \frac{3}{2}\bar{V}_{th}\rho_s\left[\frac{1}{r}\frac{\partial(\lambda_i^*,\phi^*)}{\partial(r,\theta)} + (\frac{T_{i0}'}{T^*})\frac{1}{r}\frac{\partial\phi^*}{\partial\theta}\right] + \Sigma_{\lambda_i}^* \tag{7}$$

$$\frac{3}{2}\left[\frac{\partial\lambda_e^*}{\partial t} + \mathbf{u}_{e0}.\nabla\lambda_e^*\right] + \bar{V}_{th}(\frac{N^*T_{e0}}{n_0T^*})\nabla_\parallel\xi^* = \frac{3}{2}\bar{V}_{th}\rho_s\left[\frac{1}{r}\frac{\partial(\lambda_e^*,\phi^*)}{\partial(r,\theta)} + (\frac{T_{e0}'}{T^*})\frac{1}{r}\frac{\partial\phi^*}{\partial\theta}\right]$$
$$-(\frac{N^*T_{e0}}{n_0T^*})\bar{V}_A\nabla_\parallel\rho_s^2\nabla_\perp^2\psi^* + \Sigma_{\lambda_e}^* \tag{8}$$

These equations include, within the two-fluid model, physical effects such as visco-resistive tearing, ballooning, drift-Alfvén and η_i modes. A closely related subset is used in[13].

Assuming time-independent external sources, the Σ^* quantities (ie, sources for the fluctuations) include the following type of terms: a) neoclassical perpendicular transport[14] terms; b) fluctuating divergences of parallel heat fluxes, $\mathbf{q}_{\|i,e} = -n_e\chi_{i,e}\nabla_\| T_{i,e}$, in Eqs.(7,8) ; a simple correction [16] (see Eq.(31), *loc. cit*) is applied to the parallel diffusivities for long mean-free-path: $\chi_{\|i,e} = qRv_{th}^{i,e}$; c) optional terms to represent, approximately [17], the effect of ion Landau damping, in the form of an 'effective' damping rate, $\simeq v_{th}^i k_\|$; d) turbulent diffusion terms used to prevent unphysical aliasing of long wavelengths by providing a smooth, high-k cut-off. For example, the turbulent viscosity term applying to Θ^* is of the form, $\nabla.(D_{\rm turb}\nabla_\perp\Theta^*)$, where, $D_{\rm turb} \simeq C_s\rho_s F(\Theta^*, \rho_s^2\nabla_\perp^2\psi^*)$, and F is a dimensionless, quadratic function. In regions where the turbulence is small, this nonlinear turbulent diffusivity is negligible compared to the neoclassical 'background' diffusivity. In practice, calculated values satisfy, $D_{\rm turb} \ll D_{\rm Bohm} \simeq C_s\rho_s$.

The model is completed by the transport equations satisfied by $n_0, T_{e,i0}, B_{\theta 0}, v_{\theta 0}$ and $v_{\zeta 0}$. These are obtained by averaging the exact equations with respect to the angles and including any external sources and neoclassical transport coefficients. Thus, $n_0, T_{i,e0}, B_{\theta 0}, v_{\theta 0}, E_{r0}$ satisfy:

$$\frac{\partial n_0}{\partial t} = -\frac{1}{r}\frac{\partial}{\partial r}(r\left[\Gamma_{\rm nc} + < \delta n_e \delta v_r^E >\right]) + S_p(r,t) \tag{9}$$

$$\frac{3}{2}n_0\frac{\partial T_{i,e0}}{\partial t} = -\frac{1}{r}\frac{\partial}{\partial r}(r\left[Q_{\rm nc}^{i,e} + \frac{5}{2} < \delta p_{i,e}\delta v_r^E > + Q_{\rm m}^{i,e}\right]) + P_{i,e}(r,t) \tag{10}$$

$$\frac{\partial B_{\theta 0}}{\partial t} = \frac{\partial}{\partial r}\left[\frac{c^2\eta_{\rm nc}}{4\pi}(\frac{1}{r}\frac{\partial r B_{\theta 0}}{\partial r} - \frac{4\pi}{c}j_{\rm bs})\right] \tag{11}$$

$$\frac{\partial v_{\theta 0}}{\partial t} = -\nu_{\rm nc}(v_{\theta 0} - v_{\theta \rm nc}) - \frac{1}{r}\frac{\partial}{\partial r}(r < \delta v_r^E \delta v_\theta^E >) + < \frac{\delta j_\| \delta B_r}{m_i n_0 c} > \tag{12}$$

$$E_{r0} = \frac{1}{en_0}p_{i0}' + \frac{(v_{\zeta 0}B_{\theta 0} - v_{\theta 0}B_{\zeta 0})}{c} \tag{13}$$

In Eq.(9), $\Gamma_{\rm nc}$ is obtained from neoclassical theory[14] and $< \delta n \delta v_r^E >$ $(= \Gamma_{\rm turb})$ is the (ambipolar) turbulent particle flux, where, $\delta v_r^E = -\frac{c}{B}\frac{1}{r}\frac{\partial \delta\phi}{\partial \theta}$, and the average is with respect to angles, θ, ζ, for given r, t. Since the particle source, $S_p(r,t)$ is not well-known experimentally, a simple feed-back term is used to keep the line average of $n_0(r,t)$ fixed at a specified (ie, experimental) value throughout the simulation. The energy equations for $T_{e,i}$ involve neoclassical radial heat fluxes and turbulent heat fluxes, with additional terms including electron-ion equilibration (neoclassical), ohmic and auxiliary heating sources. For simplicity, the latter are assumed to be specified functions of r. Whilst the turbulent ion heat flux, $5/2 < \delta p_i \delta v_r >$ $(= Q_{\rm turb}^i)$, is entirely advective (ie, $Q_m^i \simeq 0$), the electron turbulent radial heat flux has a term of this type and an additional 'magnetic fluctuation' term, $Q_m^e =< q_{\|e}\mathbf{b}.\mathbf{e}_r >$ of the Rechester-Rosenbluth form[16]. The energy source terms $P_{i,e}$ include Ohmic and auxiliary heating (with specified profile and strength), and classical electron ion equilibration and radiation/charge-exchange

losses (if any). At present, $B_{\theta 0}$ is evolved in CUTIE according to Eq.(11) using the neoclassical induction equation[14], neglecting 'turbulent dynamo' effects (left for future investigations), where $\eta_{\rm nc}$ is the neoclassical resistivity, and $j_{\rm bs}(r,t)$ is the bootstrap current source[14]. In the experiments simulated, there were no current drive sources, which could be included in Eq.(11), if desired. It is assumed that there are no external *poloidal* momentum sources. Averaging the poloidal component of the total momentum balance equation with respect to angles θ, ζ, Eq.(12) is obtained, where, $\epsilon = r/R$, $\nu_{\rm nc} = 0.67\epsilon^{-1}\tau_i^{-1}$, and $v_{\theta \rm nc} = -1.17(1 - 1.46\epsilon^{1/2})(\frac{cT_{i0}'}{eB})$ [18]. It expresses the balance between turbulence-driven poloidal accelerations (due to radial $E \times B$ advection and Lorentz forces) and neoclassical poloidal flow damping[14]. Since the momentum source in the toroidal direction is not well-known, the present model makes the simple assumption that $v_{\zeta 0} = v_{thi} M_a$, where the ion Mach number (M_a) is taken to be a fixed parameter. The equilibrium radial electric field, E_{r0}, is then determined by the radial component of the mean momentum balance equation for ions, Eq.(13).

The mean equations (9,10) are solved with suitable edge pedestal conditions and zero gradients at $r = 0$, starting from simple (arbitrary) Gaussian or parabolic profiles. The induction equation (Eq.(11)) is solved with the boundary conditions, $B_{\theta 0}(a) = 2I_p/ac$, $B_{\theta 0}(0) = 0$, with I_p being the specified plasma current (in cgsu). The boundary data for the fluctuating quantities at $r = 0$ follow from regularity requirements on the fields and velocities; all fluctuations vanish at $r = 0$ except for the $m = 1$ components of velocity and magnetic field. Zero values are imposed at $r = a$, but the actual plasma edge corresponds to $r/a = 0.95$.

Equations (2-6) for the fluctuations are solved by Fourier-transforming and radial finite-differencing, treating the mode coupling terms iteratively. These terms are first evaluated in position-space using a centred-differenced, conservative Jacobian scheme and then Fourier-transformed to get the (explicit) sources for the block-tridiagonal system coupling $\hat{\Theta}, \hat{\phi}, \hat{\psi}, \hat{n}$ and $\hat{\xi}$ for each pair of (m,n). Denoting by $\mathbf{X}_i(m,n,t+\Delta t)$, the column vector formed by these five Fourier components at the radial mesh point (i), the resultant system of (nonlinear) algebraic equations takes the form,

$$\mathbf{A}_i^0 \mathbf{X}_i(m,n,t+\Delta t) \;=\; \mathbf{A}_i^+ \mathbf{X}_{i+1}(m,n,t+\Delta t) + \mathbf{A}_i^- \mathbf{X}_{i-1}(m,n,t+\Delta t) + \mathbf{S}_i \quad (14)$$

where $\mathbf{A}_i^0, \mathbf{A}_i^+, \mathbf{A}_i^-$ are (5×5) complex matrices (functions of m,n,i,t) and $\mathbf{S}_i$ is a 'source' column vector including nonlinear and toroidal coupling effects as well as terms involving $\lambda_{i,e}^*$. The semi-implicit differencing scheme (centred-space, backwards time for implicit terms and centred time for the explicit ones) ensures that this block-tridiagonal system is always invertible (ie non-singular) for $\mathbf{X}_i$ at $t+\Delta t$, given the values at t and the boundary conditions. This linear system is inverted by complex block-tridiagonal, Gauss-Jordan pivoting for $-m_{\rm max} \le m \le m_{\rm max}$ and $0 \le n \le n_{\rm max}$. Reality conditions are used to determine the values for the remaining n harmonics. Having obtained $\mathbf{X}_i$, the semi-implicitly differenced, Fourier-transformed versions of Eqs.(7,8), are solved by a radial tridiagonal matrix solver for $\hat{\lambda}_{i,e}(r_i,m,n,t+\Delta t)$. The complete solution

involves two predictor-corrector iterations at each time-step. Extensive experience with both linear and nonlinear simulations[9, 10] has shown that the scheme described is stable and convergent. The prescription of the time-step is limited by accuracy considerations, with $V_A \Delta t/a \simeq 0.25$, being a typical choice. Spatial resolutions are chosen to obtain, $\Delta r \leq \rho_s$, at least, away from the cool edge.

III. Simulation results

RTP simulations: These runs, preliminary results of which were reported briefly in a UKAEA report[9], apply to the following plasma conditions[1]: $a = 0.165$m, $R = 0.72$m, $B_0 = 2.15$T, $I_p = 66$kA, $P_{\rm ECH} = 350$kW. Three cases of ECH deposition are considered (Cases A,B and E, respectively, in Fig.1a) with $\rho_{\rm dep} \equiv r_{\rm dep}/a = 0.1, 0.35, 0.55$. In all three simulation cases presented, the q profile is monotonic from $q_0 = 0.85$ to $q_a = 6$. This corresponds fairly closely to the estimated[1] profile for Case A, but is significantly different from those estimated in the other two experimental cases(*op.cit*, Fig.4). CUTIE results pertain only to the first millisecond (about 10^5 time-steps) after 'switch-on', and the q profile does not have enough time to evolve significantly away from its initial value. The experimental profiles were estimated[1] in 'steady-state', nearly 250 ms after switch-on, and are different for the three cases. For this reason, among others, the comparison between the experimental T_e profiles shown in Fig.1a (obtained in steady state) and the theoretically calculated ones (Fig.1b) is strictly qualitative. The simulations vary *only* $\rho_{\rm dep}$, keeping everything else fixed, including initial profiles of $q, n_e, T_{e,i}$, whereas, in the experiments, both $\rho_{\rm dep}$ and q_0 vary at constant total power, current, etc. The assumed power deposition profile in the simulations is of the form, $P_{\rm ECH} \simeq \exp\left[-(r - r_{\rm dep})^2/w^2\right]$, where, $w = a/7 \simeq 2.3$cm. The chosen width is nearly twice as large as in the experiment, since it was thought important to separate genuine effects of steep transport barrier formation from those due to narrow heating profiles. Subsequent calculations with the experimental width yield similar results. Gaussian initial temperature ($T_{e,i}(0) \simeq 0.8$keV) and density ($n_e(0) \simeq 5.0 \times 10^{19}$m^{-3}) profiles were used, consistent with the Ohmic state, prior to switch-on of ECH, together with randomized, small amplitude 'noise' in the initial fluctuations. A particle source profile of $S_p(x) = x(1 - 1.1x^2); x = r/a$ was used, with feed-back line-averaged density $\bar{n}_e \simeq 2.7 \times 10^{19}$m^{-3}, close to experiment. Calculations used a resolution of 100 radial mesh points, 32 poloidal and 16 toroidal harmonics($\Delta r \simeq \rho_s/2$, $\Delta t \simeq 5$ ns, $V_A \simeq 5 \times 10^6$m.s^{-1}). Higher resolution (100x64x32, 100x64x64) calculations have also been carried out for shorter total time lengths, and show no significant differences apart from better definition of the fine-scales.

In Fig.1b, the calculated T_e profiles in the three cases are shown, together with the q profile. Comparison with experiment (Fig.1a) shows that the calculated T_e profiles exhibit features similar to the experimentally measured ones, particularly in Cases A and B, where the difference between model and experimental q profiles is not large. Even in case E, where the difference is greatest, the basic features of the profiles are

reproduced. In particular, the location of the transport barriers, the off-axis maxima and the corrugations (ie, relatively high local gradient features) are captured qualitatively. The experimental profiles show stronger corrugations, possibly indicating inadequate resolution at the higher wave numbers in the simulations. The corrugations in $v_\theta^E \equiv -cE_r/B, j_{bs}$ are more prominent, as shown in Fig.5, for Case B. The plasma current density, j_z is less corrugated, as expected, from the properties of Eq.(11). Although these quantities are strictly not measured on RTP, it is known from many other experiments[2, 4, 5] that the radial electric field has the predicted type of 'corrugated' structure implying poloidal 'jets' in the electric drift (see, for example, Fig.3, given in Gormezano's paper[2]). For RTP conditions, the radial electric field is primarily determined by the ion pressure gradient and little influenced by the 'zonal flow', $v_{\theta 0}$, driven by Reynolds stresses. CUTIE is provided with a diagnostic post-processor capable of making movies of all relevant turbulence and profile properties. In Case B, for example, these movies show that about 50 μs from the start, a $(3,2)$ resonant mode spontaneously grows (saturating later) and rapidly steepens the gradient near this rational surface, inboard of it. A similar, though weaker effect, is seen at the $(2,1)$ resonance, in broad agreement with the phenomenological model of [1]. After this rapid initial phase involving an inverse cascade, the profiles and the turbulence evolve corrugations more slowly over a longer period[9]. In general, the typical radial wavenumber, $k_r \geq k_\theta \simeq m/a$. Core mode rotation is often counter to the edge mode rotation, with intermittent locking and 'bursting' reversals. All three cases exhibit similar features (though different modes are involved in each case). The low mode number part of the fluctuation spectrum is excited by an inverse cascade [11] and nonlinear instability[13] even when the runs are started with high mode numbers. In general, the initial data on the turbulence play no role in the final saturated spectra, as one expects in a strongly driven, dissipative system. In all three cases, the central temperature dip is associated with a strong outward advective turbulent flux *inboard* of the barriers. Such a dip is inconsistent with a purely local diffusive transport, although not with any fundamental principle such as the second law of thermodynamics (the system considered is everywhere driven hard, and is far from equilibrium).

JET-like simulations: Realistic, global, JET simulations pose several problems at present, since the periodic cylinder model is inadequate for JET conditions, due to shaping. Furthermore, $\rho_s/a = \rho_* \simeq 4 \times 10^{-3}$, and this makes adequate radial resolution impractical. The JET time-scale is long (several hundred milliseconds), whereas, computationally it is not feasible to make runs for much longer than 2ms. For these reasons, the calculations presented should be viewed as first attempts to model qualitatively, the initial transient physics of ITBs in JET. The results discussed below are from a sequence of four runs continued for a total time of 1.5 ms (45000 time-steps). These high resolution ($100 \times 64 \times 32$; $\Delta t \simeq 30$ns) runs were made with parameters suggested by JET shot #49006: $R = 3$m,$a = 1.25$m,$B_0 = 2.6$T, $P_{aux} \simeq 15$MW, $I_p \simeq 2.3$MA, $\bar{n} \simeq 1.5 \times 10^{19}\mathrm{m}^{-3}$, $q_0 \simeq 2.2$ (somewhat lower field and current as compared with #46727, shown in Fig. 2), $M_a = 0.3$. The power deposition profiles were assumed

parabolic and equal amounts of power were applied to the two species. The particle source profile was chosen as for RTP.

The experimental (from charge exchange diagnostics) T_i profile close to the time of barrier formation is shown in Fig.6a, and the calculated profile in Fig.6b. The main transport barrier at the end of the simulation (starting with initial Gaussian profiles and random fluctuations) forms near $r/a \simeq 0.8$ in T_i and weaker, inner barriers are also plainly visible (Fig. 6b). The simulated profile is qualitatively similar to the experimental profile. Figures 7a,b, compare the observed (from the LIDAR diagnostic) and the calculated T_e profiles, again demonstrating qualitative agreement. In view of many uncertainties relating to sources and diagnostics, this agreement is encouraging. The experimental (also from LIDAR) and the computed n_e profiles are shown in Figs.8a,b. Once formed, the barriers evolve slowly in time and have a tendency to reduce q' locally. The secondary, weaker barriers, form at other low order rational surfaces.

The computed $\mathbf{E} \times \mathbf{B}$ poloidal flow (Fig. 9) reveals highly sheared, 'jet-like' mesoscale structures in the barrier zone (compare with Fig.3). The JET simulations are influenced both by the toroidal flow due to the beams and the turbulence–driven, 'zonal' (poloidal) flows[8]. Thus all the terms in Eq.(13) seem to be important under these conditions. Figures10a,b shows an instantaneous snap-shot of the computed radial and poloidal $\mathbf{E} \times \mathbf{B}$ velocity fluctuations, revealing 'streamers' ($m = 7$ and higher harmonics) and ballooning micro-turbulence associated with an $m = 8, n = 3$ resonance, close to the barrier. The radial wavelengths are noticeably shorter than poloidal ones, as noted earlier. Movies also show that current filamentation occurs, suggesting that magnetic fluctuations play a key dynamical role. Current effort is directed towards increasing processing power using parallel processing variants of CUTIE to carry out more realistic simulations over longer time-scales with better resolution.

IV. Summary and conclusions

Global, nonlinear, electromagnetic simulations of tokamak turbulence with special reference to internal transport barriers in RTP[1] and JET[2] have been presented. The model, although considerably simplified, seems to be able to capture the main qualitative characteristics of transport barriers in both experiments, although the heating schemes and conditions are very different. The turbulence exhibits 'self-organizational' tendencies noted by earlier workers[11, 13] typical of driven, dissipative nonlinear systems. The low (m, n) spectrum observed in the simulations is associated with *rational* q surfaces and relatively long wave-length electromagnetic modes. It plays a key role in the dynamics. These modes are qualitatively similar to 'snakes'[2] and filaments[12] observed in experiment. Filaments are nonlinearly saturated helical disturbances, as opposed to 'corrugations', which are essentially $m = n = 0$, time-dependent, high local radial gradient features. Both types of structures exist and interact in complex ways throughout the evolution. It is apparent that fine-scale, intermittent turbulence

is generated through nonlinear and toroidal mode couplings and secondary instabilities (direct cascade). Furthermore, turbulent fluxes (eg, $< \delta n_e \delta v_r^E >$) varying rapidly in space and time (as in [13, 19]) can 'corrugate' profiles influencing the local gradients of both magnetic (q', j') and electric fields (E_r'). These in turn, drive and damp the turbulence in a relaxation process. Thus, there clearly exist two separate feed-back loops governing the co-evolution and interaction of electromagnetic plasma turbulence and profiles, associated with E_r[8] and $j_{\rm bs}$[7], respectively. The resulting nonlinear dynamics[11, 13] involves complex mode rotation, current filaments('snakes'), internal mode-locking, relaxation oscillations, avalanches[19], and intermittent bursts of high k, ω turbulence.

The above features are readily visualized in movies made from the simulations, and are broadly reproducible, irrespective of the initial conditions. They appear to be general, model-independent features of low-frequency, nonlinear, electromagnetic, two-fluid plasma turbulence in tokamaks. The transport barriers themselves are regions of high profile gradients which appear to form spontaneously in association with rational q surfaces in a self-organized process in which corrugations of both radial electric field shear and bootstrap currents are involved. The results presented in this paper suggest that ITBs can be modelled from first principles with a two-fluid direct numerical simulation code, provided due account is taken of the global, nonlinear, and electromagnetic aspects of the problem. Future work will be aimed at establishing the essential qualitative and quantitative behaviour of ITBs, including their scaling properties, using improved versions of CUTIE to interpret the data available from a variety of steady-state and transient experiments.

Acknowledgements: I am especially grateful to Marco de Baar, Michele Romanelli, Vassili Parail, Dick Hogeweij, Niek Lopes Cardozo, Marc Beurskens, Howard Wilson, Jack Connor and Terry Martin for their invaluable help and advice. This research was jointly funded by the UK Dept. of Trade and Industry and Euratom.

References

[1] G.M.D. Hogeweij *et al*, Nucl. Fusion, **38**, 1881 (1998). See also the review by N.Lopes Cardozo *et al*, Physicalia, **20**, p. 169 (1998) and *Electron Transport Barriers in Tokamak Plasmas*, M.R. de Baar, Ph.D Thesis (Technical Univ. Eindhoven, 1999).

[2] C. Gormezano, Plasma Phys. Control. Fusion **41**, B367 (1999); also, M. Keilhacker *et al*, Plasma Phys. Control. Fusion **41**, B1 (1999) and C. Gormezano *et al*, Phys. Rev. Lett. **80**, 5544 (1998).

[3] Y. Kamada and the JT-60 Team, Plasma Phys. Control. Fusion **41**, B77 (1999).

[4] M.G. Bell *et al*, Plasma Phys. Control. Fusion, **41**, A719 (1999).

[5] E.J. Strait *et al*, Phys. Rev. Lett. **75**, 4417 (1995), also, R. Moyer *et al*, Phys. Plasmas, **2** 2397 (1995).

[6] W. Horton *et al*, Phys. Plasmas **5**, 3910 (1998).

[7] K. Itoh, S-I. Itoh and A. Fukuyama, *Transport and Structural Formation in Plasmas*, Inst. of Phys., Bristol, (1999).

[8] K.H. Burrell, Science, **281**, 1816 (1998).

[9] A. Thyagaraja, in *Theory of Fusion Plasmas*, Proc. Varenna-Lausanne International Workshop, 155 (1996). See also Proc. 26th Euro. Phys. Soc. Conf. Maastricht, P.1009, (1999), and UKAEA Fusion Report, FUS 419, (1999).

[10] A. Thyagaraja, Plasma Phys. Control. Fusion **36**, 1037 (1994) and A. Thyagaraja *et al*, Proc. 24th Euro.Phys. Soc. Conf. Berchtesgaden, **21A**, 277, (1997).

[11] A. Hasegawa and M. Wakatani, Phys. Rev. Letts. **59**, 1581, (1987).

[12] M. Beurskens, *Filamentation of tokamak plasmas*, Ph. D thesis (and references therein), Technical University of Eindhoven (1999).

[13] A. Zeiler, J.F. Drake and B.N. Rogers, Phys. Rev. Letts., **84**, 99 (2000)

[14] R.D. Hazeltine and J.D. Meiss, *Plasma Confinement*, Addison-Wesley, New York, (1992).

[15] R.D. Hazeltine and J.D. Meiss, Physics Reports, **121**, 1, (1985).

[16] A. Thyagaraja, I.L. Robertson and F.A. Haas, Plasma Physics and Control. Fusion, **27**, 1217, (1985).

[17] R.J. Goldston and P.H. Rutherford, *Introduction to Plasma Physics*, Institute of Physics Publishing, Bristol, 97, (1995).

[18] F.L. Hinton and M.N. Rosenbluth, Plasma Physics and Control. Fusion, **41**, A653, (1999).

[19] X. Garbet and R.E. Waltz, Phys. Plasmas, **5**, 2836, (1998).

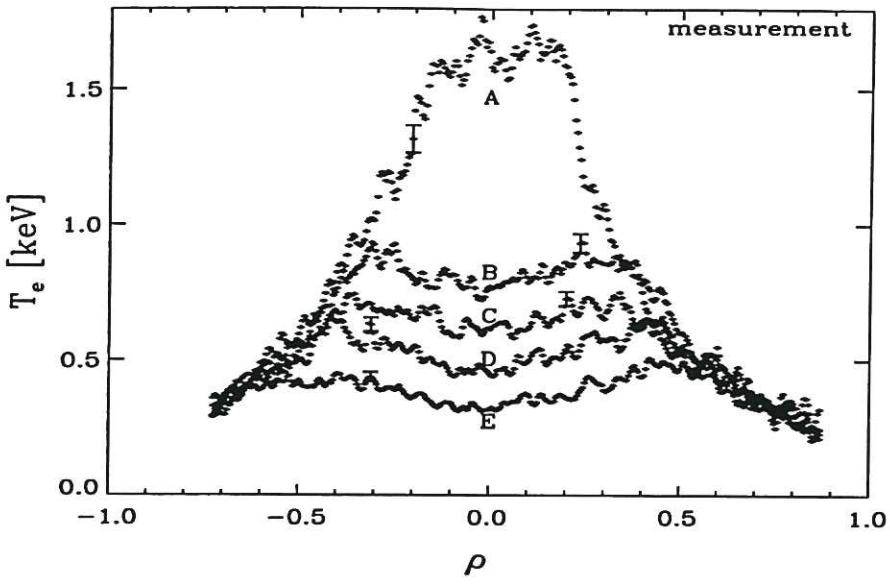

Fig.1a Measured T_e profiles in RTP[1] (see text for details)

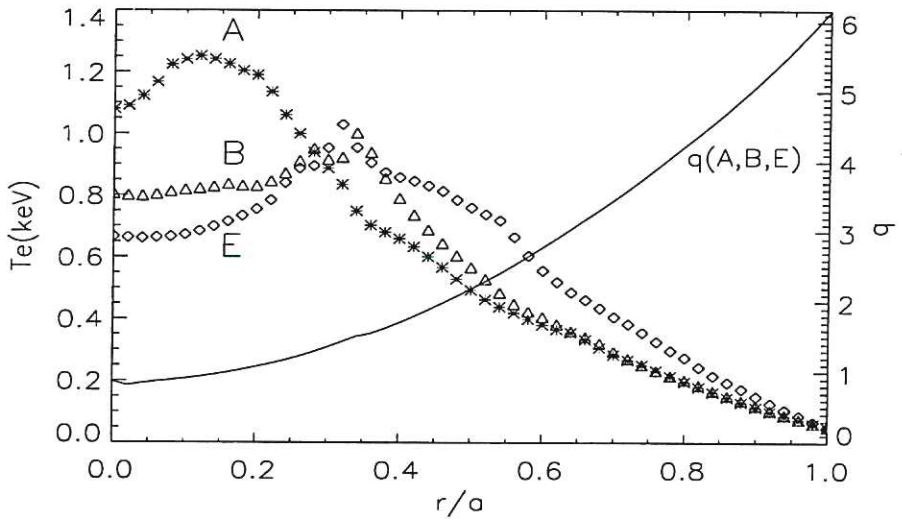

Fig.1b Calculated T_e and q (Cases A,B,E)

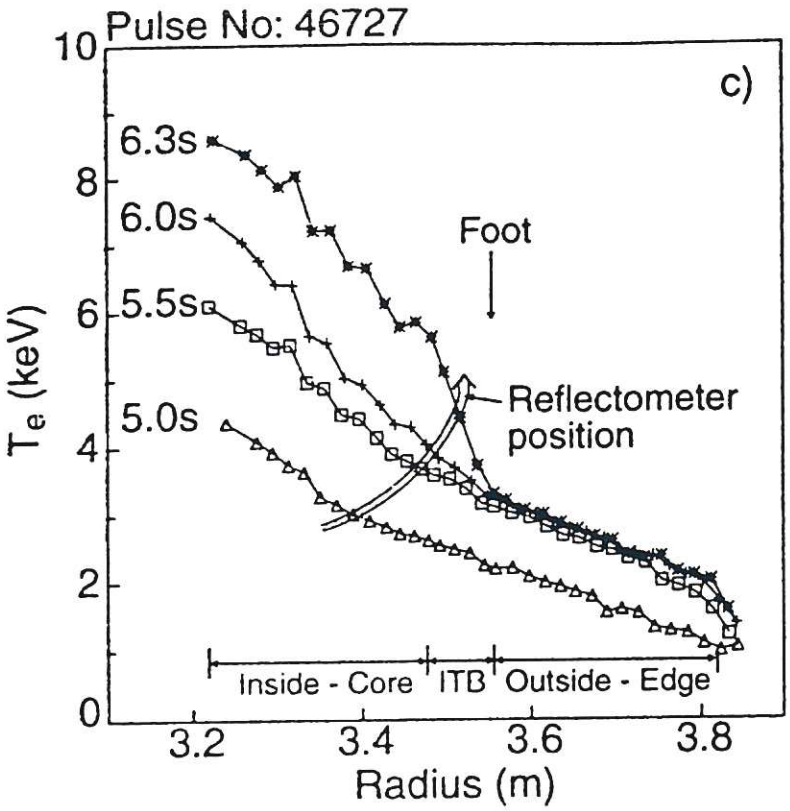

Fig.2 Measured T_e profiles, JET#46727[2]

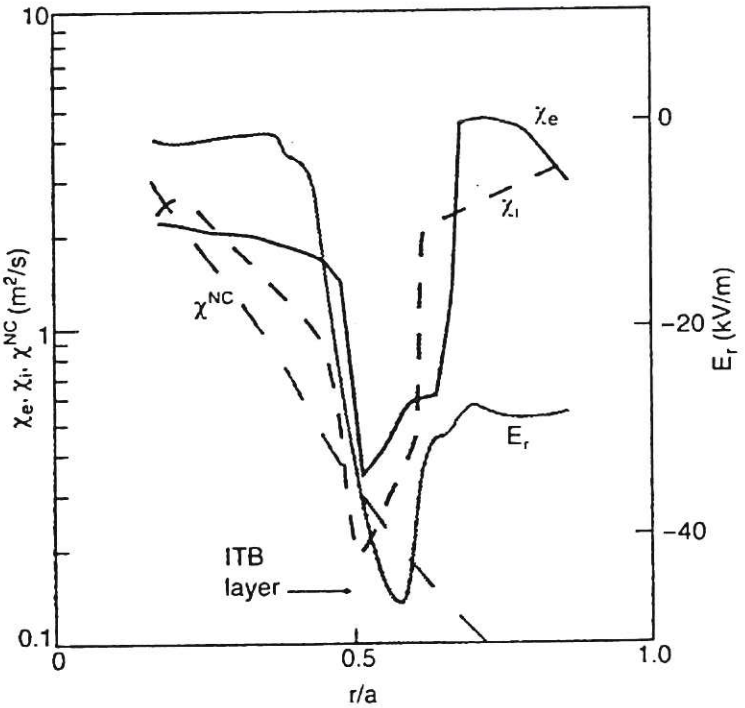

Fig.3 ITB in JT-60U showing, $E_r, \chi_{\mathrm{i,e}}, \chi^{\mathrm{NC}}$

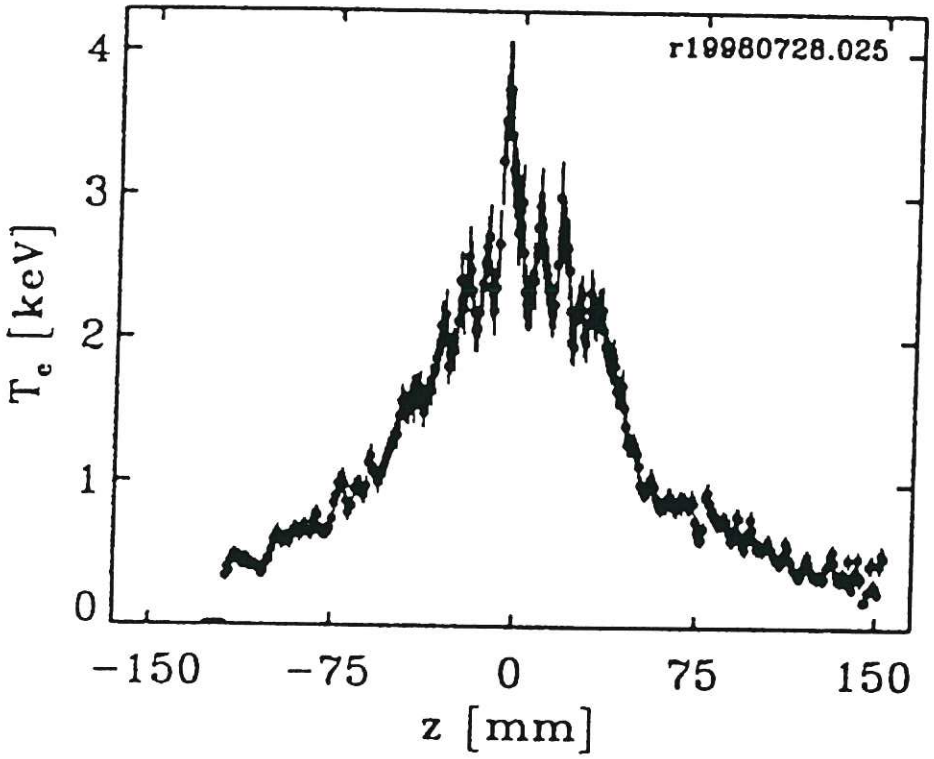

Fig.4 Filamented T_e profiles in RTP

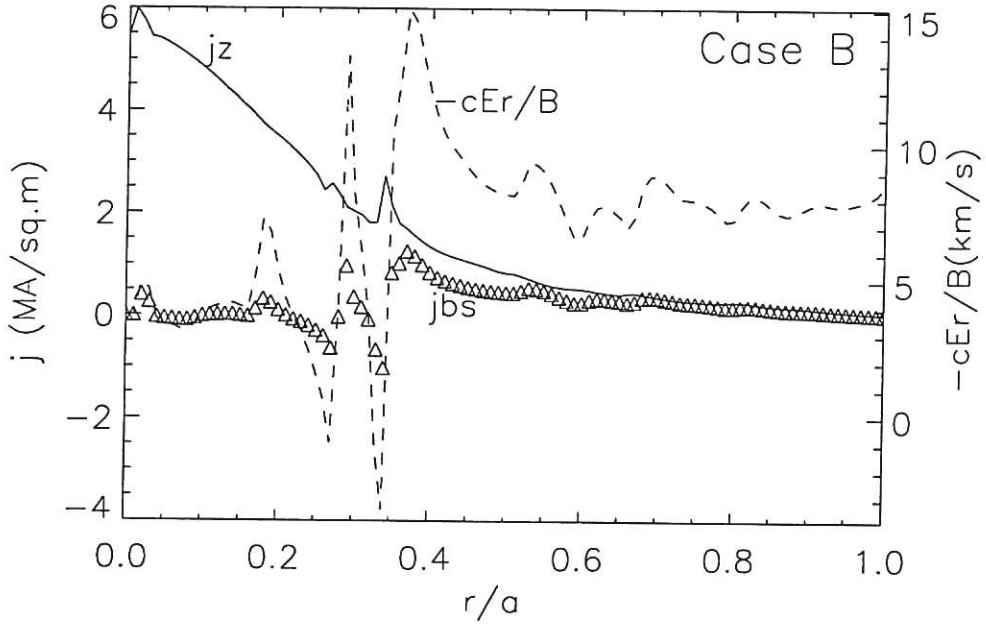

Fig.5 Corrugations in j_z, $-cE_r/B$ and j_{bs} (RTP- Case B)

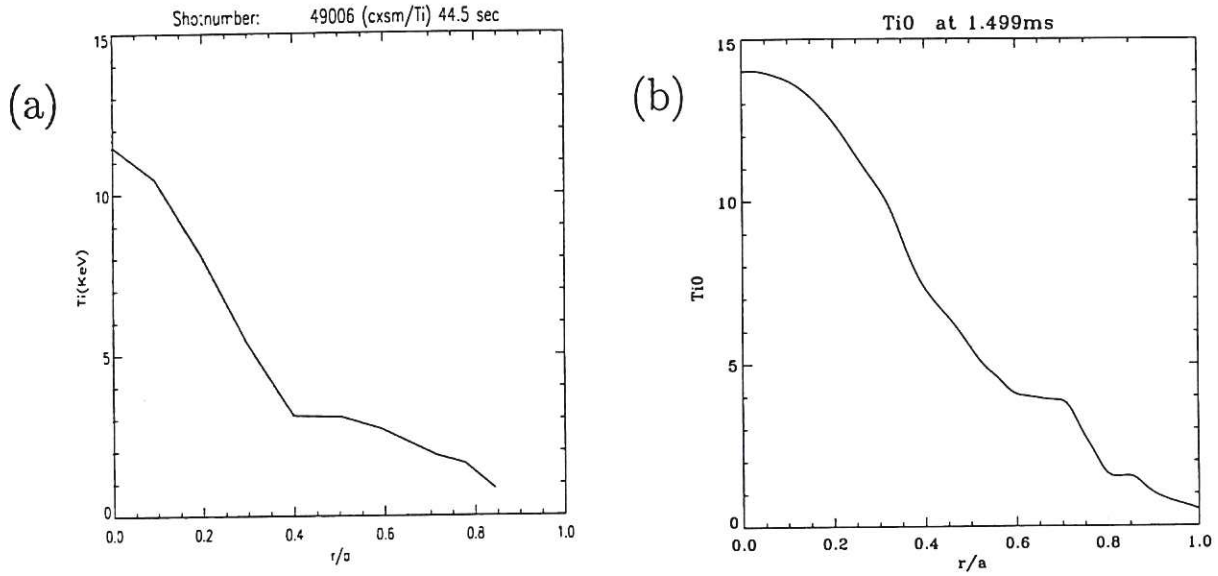

Fig.6 (a) Experimental and (b) calculated T_i (keV) profiles (JET #490(

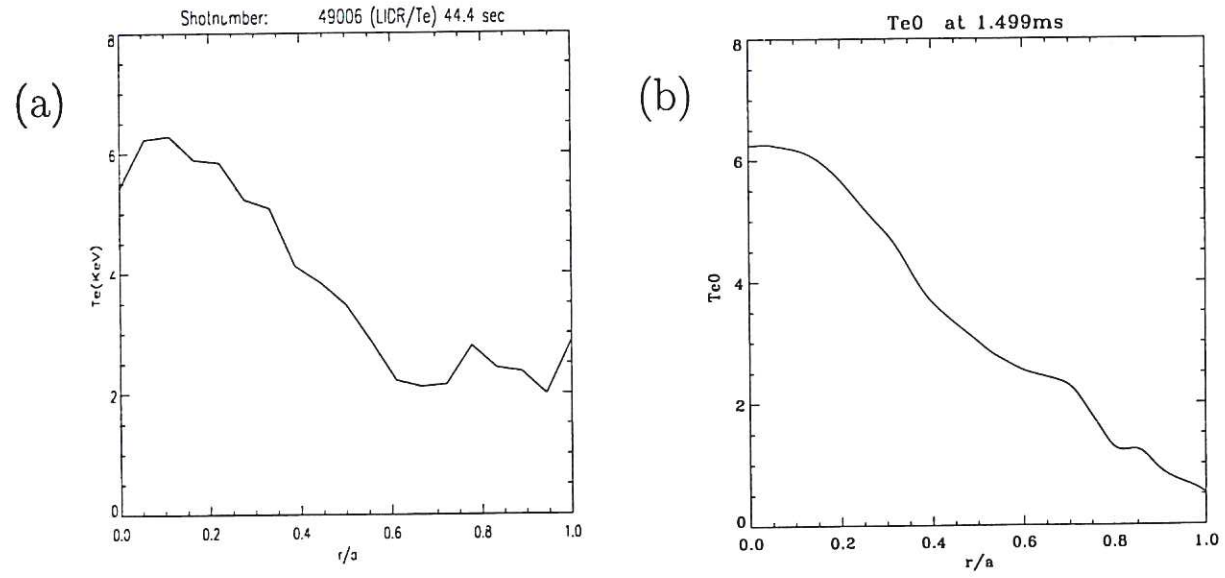

Fig.7 (a)Experimental and (b) calculated T_e (keV) profiles (JET #490(

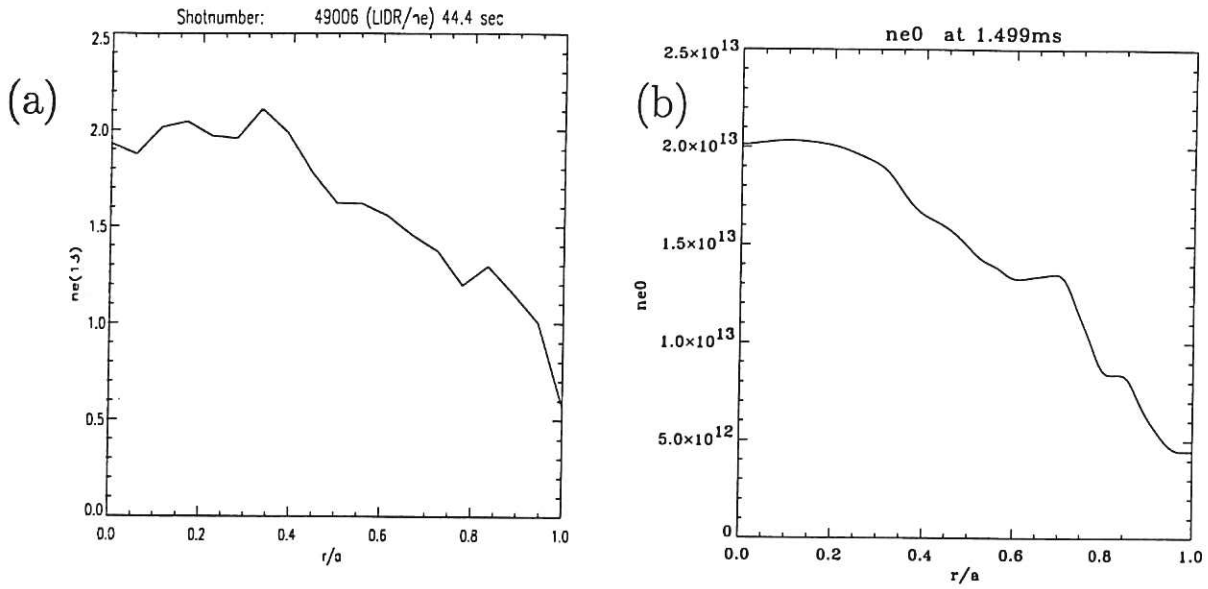

Fig.8 (a) Experimental and (b) calculated n_e (cm^{-3}) profiles in JET

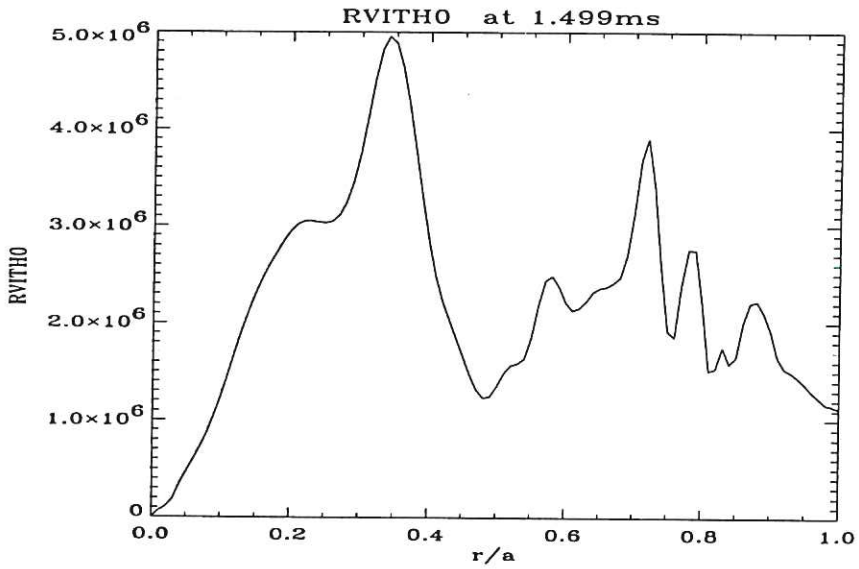

Fig.9 Calculated $-cE_r/B$(cm/s) flow in JET

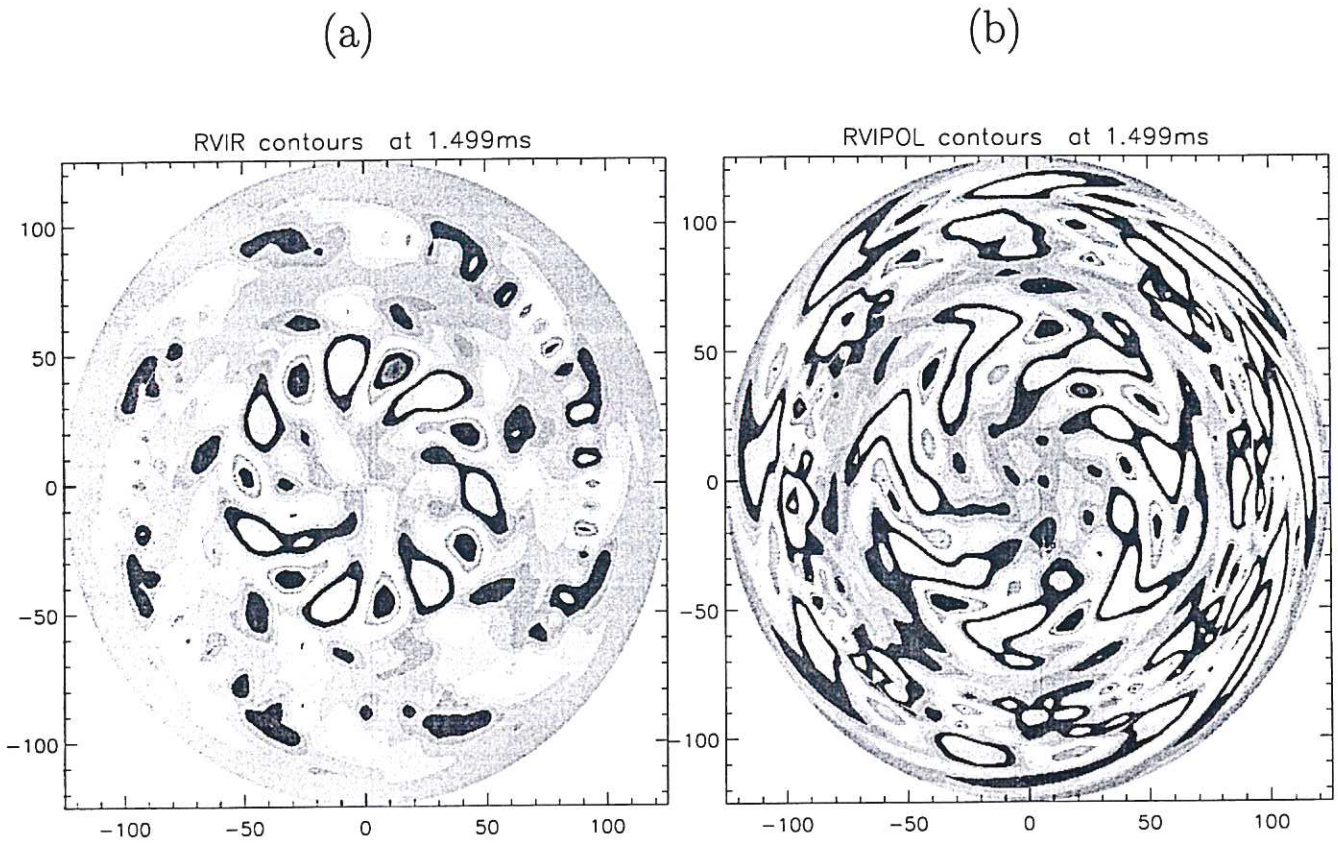

Fig.10 Computed contours of: (a) $\delta v_r = -\frac{c}{B}\frac{1}{r}\frac{\partial \delta\phi}{\partial \theta}$ and (b) $\delta v_\theta = \frac{c}{B}\frac{\partial \delta\phi}{\partial r}$

UKAEA FUS 433

EURATOM/UKAEA Fusion

The resistive wall instability and critical flow velocity

C N Lashmore-Davies

September 2000

EURATOM/UKAEA Fusion Association

Culham Science Centre, Abingdon
Oxfordshire, OX14 3DB
United Kingdom
Telephone +44 1235 463357
Facsimile +44 1235 463647

The Resistive Wall Instability and Critical Flow Velocity

C N Lashmore-Davies

UKAEA Fusion, Culham Science Centre, Abingdon, Oxon, OX14 3DB, UK

Abstract

A cylindrical model with an equilibrium surface current and a uniform equilibrium plasma flow velocity parallel to the axis of the cylinder is used to investigate resistive wall instability. This system can be unstable to the ideal, external kink mode, which can be stabilised by the presence of a perfectly conducting wall. This is the classic condition for the resistive wall instability and the effect of a plasma flow velocity on this mode is explored. It is noted that a stable kink mode, Doppler shifted by the flow velocity, can pass through zero frequency for a velocity which depends on the marginal condition for the external kink instability. The passage through zero frequency is the condition for the kink mode to carry negative energy. It is shown how this mode implies a critical flow speed at which the resistive wall mode is further destabilized, with a growth rate inversely proportional to the square root of the wall time. Under these circumstances, the resistive wall mode behaves more like an ideal instability. All flow velocities are shown to be potentially destabilizing and the flow velocity can produce a resistive wall instability even when the plasma is stable to the external kink mode in the absence of a wall. At velocities well above the critical flow speed, the resistive wall growth rate is much reduced (inversely proportional to the wall time and to the flow speed).

I INTRODUCTION

With the advent of advanced tokamaks with improved confinement there has been renewed interest in resistive wall instability[1] since this would be a threat to the success of these devices. The recent observation[2] of an extension of the wall stabilised lifetime of DIII-D[3] to more than 30 times the resistive wall time in the presence of toroidal rotation has also focussed attention on the effect of rotation on resistive wall instability. An early treatment of the effect of rotation on resistive wall modes was given by Gimblett[4] who later considered the effect of a secondary wall[5] rotating relative to the first wall. Since this early work several authors[6–12] have analyzed the effect of rotation with the aim of identifying a stabilizing effect due to rotation.

Recently, Wesson[13] discussed a very simple model in order to clarify the role of a flow velocity on the resistive wall instability. For a uniform incompressible slab of fluid in the presence of a uniform flow velocity along a uniform magnetic field it was shown that the flow velocity resulted in a resistive wall instability if $v_0 > \sqrt{2}c_A$ where v_0 is the flow speed and c_A the Alfvén speed. An extension of this model to a compressible plasma[14,15] showed that, in addition to this instability, a second resistive wall instability occurred when $v_0 > c_S$ where c_S is the sound speed, and for low beta conditions, $c_S \ll c_A$. However, these very simple models are not relevant to a tokamak. The most important feature missing from these models is free magnetic energy. The purpose of this paper is to analyse the effect of a flow velocity along the equilibrium magnetic field on resistive wall instability for a model which contains free magnetic energy. The characteristic feature of the resistive wall instability of a magnetically confined plasma is that in the absence of a wall the plasma is unstable to an ideal kink mode which is stabilized by the presence of a perfectly conducting wall close to the plasma-vacuum boundary. When the perfectly conducting wall is replaced by one with finite resistivity the plasma becomes unstable to the resistive wall mode.

In order to keep the analysis as simple as possible a cylindrical model with a surface current at the plasma-vacuum boundary is used. A uniform plasma flow velocity along the axis of the cylinder is assumed which is parallel to the equilibrium magnetic field in the plasma. The motivation for this study is to elucidate the effect of a flow velocity on the resistive wall instability of the type defined at the end of the previous paragraph. It is also of interest to discover whether there are any critical values of the flow velocity for the instability. The outline of the paper is the following. In Section II the cylindrical model is defined and the equations of ideal magnetohydrodynamics (MHD) are used to obtain a second order equation for perturbations to the equilibrium state. The boundary conditions at the plasma-vacuum interface at $r = a$ and at the wall at $r = b$ are given in Section III and used to obtain the dispersion relation. Solutions of the dispersion relation are given in Section IV and a summary and conclusions are given in Section V.

II THE CYLINDRICAL MODEL

The starting point for the analysis in this paper is Ref 16 in which an infinitely long cylinder of plasma, of radius a, with uniform density, pressure, and magnetic field is considered. The

confining magnetic field is produced by a surface current J_0 flowing parallel to the axis of the cylinder at the plasma-vacuum boundary. Thus

$$\boldsymbol{J}_0 = \hat{z} J_0 \delta(r-a) \tag{1}$$

where $\delta(x)$ is the Dirac δ-function. The magnetic field resulting from this current is

$$B^p_{0\theta}(r) = 0 \quad , \quad 0 \le r < a$$

$$B^v_{0\theta}(r) = \frac{\mu_0 a}{r} J_0 \quad , \quad a \le r$$

There is also a constant axial magnetic field in both plasma, B^p_{0Z}, and vacuum B^v_{0Z}. Since there is no poloidal surface current it is assumed that $B^p_{0Z} = B^v_{0Z}$. The equilibrium pressure balance at $r = a$ gives

$$p_0 = \frac{\left(B^v_{0\theta}(a)\right)^2}{2\mu_0} \tag{2}$$

In Ref 16 the plasma is assumed to be stationary in the equilibrium state and to be surrounded by a vacuum which extends to infinity. In this paper, the plasma is assumed to have a uniform flow velocity v_0 parallel to the axis. In addition, there is a thin wall, of thickness Δ, having finite resistivity and positioned at $r = b$, concentric with the plasma cylinder. In the regions between the plasma and the wall and beyond the wall ($r > b$) there is a vacuum.

Perturbations about this equilibrium are described by the linearized equations of ideal MHD. In the presence of a uniform axial flow of the plasma, the linearized equations are

$$\rho_0 \frac{\partial \mathbf{v}_1}{\partial t} + \rho_0 (\boldsymbol{v}_0 \cdot \boldsymbol{\nabla}) \boldsymbol{v}_1 = -\boldsymbol{\nabla} p_1 - \boldsymbol{\nabla} \frac{(\boldsymbol{B}_0 \cdot \boldsymbol{B}_1)}{\mu_0} + \frac{1}{\mu_0} (\boldsymbol{B}_0 \cdot \boldsymbol{\nabla}) \boldsymbol{B}_1 \tag{3}$$

$$\frac{\partial \boldsymbol{B}_1}{\partial t} = \boldsymbol{\nabla} \times (\boldsymbol{v}_1 \times \boldsymbol{B}_0) + \boldsymbol{\nabla} \times (\boldsymbol{v}_0 \times \boldsymbol{B}_1) \tag{4}$$

$$\frac{\partial \rho_1}{\partial t} + \rho_0 \boldsymbol{\nabla} \cdot \boldsymbol{v}_1 + (\boldsymbol{v}_0 \cdot \boldsymbol{\nabla}) \rho_1 = 0 \tag{5}$$

Assuming an isothermal equation of state, $p_1 = c_S^2 \rho_1$, where c_S is the sound speed $(p_0/\rho_0)^{1/2}$, and that all perturbations vary as $f(r) \exp i(kz + m\theta - \omega t)$, the perturbed variables can be expressed in terms of v_{1Z}. Carrying out this elimination, the following second order equation for v_{1Z} is obtained

$$\frac{d^2 v_{1Z}}{dr^2} + \frac{1}{r} \frac{dv_{1Z}}{dr} - \alpha^2 v_{1Z} - \frac{m^2}{r^2} v_{1Z} = 0 \tag{6}$$

where

$$\alpha^2 = \frac{\left(k^2 - \frac{\bar{\omega}^2}{c_A^2}\right)\left(k^2 - \frac{\bar{\omega}^2}{c_S^2}\right)}{\left(k^2 - \frac{\bar{\omega}^2}{c_A^2} - \frac{\bar{\omega}^2}{c_S^2}\right)} \tag{7}$$

and $\bar{\omega} = \omega - kv_0$. The solution of Eq (6) which is finite at $r = 0$ is

$$v_{1Z} = CI_m(\alpha r) \tag{8}$$

where I_m is a modified Bessel function of the first kind. In addition, p_1, v_{1r} and B_{1Z} are also required. These variables can be expressed in terms of v_{1Z} and are

$$p_1 = \frac{\bar{\omega}\rho_0}{k} v_{1Z} \tag{9}$$

$$v_{1r} = -\frac{i}{k} \frac{\left(k^2 - \frac{\bar{\omega}^2}{c_S^2}\right)}{\alpha^2} \frac{dv_{1Z}}{dr} \tag{10}$$

$$B_{1Z} = \frac{kB_{0Z}}{\bar{\omega}} \frac{(\bar{\omega}^2 - k^2 c_S^2)}{k^2 c_S^2} v_{1Z} \tag{11}$$

III THE BOUNDARY CONDITIONS

The perturbations in the plasma must be matched to the corresponding perturbations in the vacuum region. The perturbed magnetic field in vacuum is given by $\boldsymbol{B}_1^v = \boldsymbol{\nabla}\psi$. In the region $a < r < b$, ψ is given by

$$\psi(r) = DK_m(kr) + FI_m(kr) \tag{12}$$

where $I_m(kr), K_m(kr)$ are modified Bessel functions of the first and second kinds respectively. For $r > b$,

$$\psi(r) = EK_m(kr) \tag{13}$$

which satisfies the condition that $\psi \to 0$ as $r \to \infty$. The boundary conditions at the thin resistive wall[4] at $r = b$ are:

B_{1r}^v is continuous, and

$$\left.\frac{dB_{1r}^v}{dr}\right|_b^{b+\Delta} = -\frac{i\omega}{c_W} B_{1r}^v(b) \tag{14}$$

where $c_W = (\mu_0 \sigma \Delta)^{-1}$, with Δ the thickness of the resistive wall and σ its conductivity.

Substituting Eqs (12) and (13) into these two boundary conditions, and eliminating the constants E and F in favour of D, ψ, given in Eq (12), can be written as

$$\psi(r) = DK_m(kr) + \frac{i\omega (K_m'(kb))^2 DI_m(kr)}{\{kc_W \left[I_m''(kb)K_m'(kb) - K_m''(kb)I_m'(kb)\right] - i\omega K_m'(kb)I_m'(kb)\}} \tag{15}$$

where a single prime denotes the first radial derivative of the corresponding Bessel function and a double prime the second radial derivative.

In order to eliminate the two remaining constants, two further boundary conditions are required. These are both obtained at the plasma vacuum interface at $r = a$. The first

condition is obtained from the continuity of the total pressure which can be obtained by integrating the radial component of Eq (3) across the plasma vacuum boundary, giving

$$p_1(a) + \left.\frac{B^p_{0Z}B^p_{1Z}}{\mu_0}\right|_a = \left.\frac{B^v_{0Z}B^v_{1Z}}{\mu_0}\right|_a + \left.\frac{B^v_{0\theta}B^v_{1\theta}}{\mu_0}\right|_a + \left.\frac{iB^v_{0\theta}}{\mu_0}\frac{dB^v_{0\theta}}{dr}\frac{v_{1r}}{\bar{\omega}}\right|_a \tag{16}$$

where the third term on the right-hand-side of Eq (16) results from evaluating the equilibrium magnetic pressure at the perturbed surface (see, for example Ref 18). The second boundary condition at the plasma vacuum boundary can be written[18]

$$B^v_{1r}(a) = i\left(\frac{m}{a}B^v_{0\theta}(a) + kB^v_{0Z}\right)\frac{iv_{1r}}{\bar{\omega}} \tag{17}$$

Substituting Eqs (8) - (11) and Eq (15) into Eqs (16) and (17) the dispersion relation for the modes of oscillation of a cylindrical plasma with uniform flow, a surface current and a thin resistive shell at $r = b$ is

$$\frac{\bar{\omega}^2 c_S^2}{(\bar{\omega}^2 - k^2c_S^2)} + c_A^2 = \frac{I'_m(\alpha a)}{\rho_0\mu_0\alpha I_m(\alpha a)}\left\{\frac{(B^v_{0\theta}(a))^2}{a} + \left(kB^v_{0Z} + \frac{m}{a}B^v_{0\theta}\right)^2 \times \right. \tag{18}$$

$$\left. \times \frac{\left\{[K_m(ka)I'_m(kb) - I_m(ka)K'_m(kb)]\,K'_m(kb) + \frac{ikc_W}{\omega}\,[I''_m(kb)K'_m(kb) - K''_m(kb)I'_m(kb)]\,K_m(ka)\right.}{\left\{[K'_m(ka)I'_m(kb) - I'_m(ka)K'_m(kb)]\,kK'_m(kb) + \frac{ikc_W}{\omega}\,[I''_m(kb)K'_m(kb) - K''_m(kb)I'_m(kb)]\,kK'_m(ka\right.}\right\}$$

Within the limitations of the present sharp boundary, surface current model, Eq (18) is the most general dispersion relation. It describes all the modes of the system, namely, shear Alfvén waves, fast and slow magnetosonic waves and kink modes. Solutions of Eq (18) will now be obtained for various limiting cases.

IV SOLUTIONS OF THE DISPERSION RELATION

In order to make contact with earlier work consider the case when the wall at $r = b$ is a perfect conductor, ie $c_W \to 0$. In the limit $b \to \infty$, Eq (18) is then identical to Eq (11) of Shafranov[16] for the equilibrium assumed here and taking $v_0 = 0$.

Since the main aim of the present paper is to analyse the effect of a flow velocity on resistive wall modes attention will be concentrated on the kink modes. For this purpose it is sufficient to consider the incompressible approximation to Eq (18), obtained by letting $c_S \to \infty$, giving

$$\bar{\omega}^2 = k^2c_A^2 - \frac{kI'_m(ka)}{\rho_0\mu_0 I_m(ka)}\left\{\frac{(B^v_{0\theta}(a))^2}{a} + \left(kB^v_{0Z} + \frac{m}{a}B^v_{0\theta}\right)^2 \frac{K_m(ka)\left[1 - \frac{I_m(ka)K'_m(kb)}{K_m(ka)I'_m(kb)}\right]}{kK'_m(ka)\left[1 - \frac{I'_m(ka)K'_m(kb)}{K'_m(ka)I'_m(kb)}\right]}\right\} \tag{19}$$

where, for the moment, it is still assumed that $c_W = 0$ and $\alpha \to k$ when $c_S \to \infty$. In the long wavelength limit, $ka \ll 1$, $kb \ll 1$, Eq (19) reduces to

$$\bar{\omega}^2 = k^2 c_A^2 + \frac{\left(kB_{0Z}^v + \frac{m}{a}B_{0Z}^v\right)^2}{\rho_0\mu_0}\frac{\left[1+\left(\frac{a}{b}\right)^{2m}\right]}{\left[1-\left(\frac{a}{b}\right)^{2m}\right]} - \frac{(B_{0\theta}^v(a))^2}{\rho_0\mu_0}\frac{m}{a^2} \tag{20}$$

Again, in the limit $b \to \infty$, and taking $v_0 = 0$, Eq (20) gives the well known dispersion relation for external kink modes (see for example, Ref 18). The kink mode is unstable for $m = 1$ when $-mB_{0\theta}^v/(aB_{0Z}^v) < k < 0$. For $m = 0, 2$ the external kink is marginally stable and for all higher m it is stable.

For the later discussion of resistive wall modes it is helpful to review the corresponding properties of kink modes when the perfectly conducting wall is at a finite distance from the plasma. The $m = 1$ mode is still unstable but the band of unstable wave numbers is reduced to $-B_{0\theta}^v/aB_{0Z}^v < k < -B_{0\theta}^v(G-1)/(aB_{0Z}^v(G+1))$ where $G \equiv [1+(a/b)^{2m}]/[1-(a/b)^{2m}]$. For this case the $m = 2$ mode is stable and does not reach the marginal condition. However, it is instructive to obtain the frequency of the $m = 2$ mode. This is done for the wave number k which minimises the first two terms on the right-hand-side of Eq (20). The resulting value of k is $-2B_{0\theta}^v G/aB_{0Z}^v(1+G)$. Using this value (for k) in Eq (20) the solution for $\bar{\omega}$ is given by

$$\bar{\omega}^2 = \frac{4}{a^2}\frac{(B_{0\theta}^v)^2}{\rho_0\mu_0}\frac{(G-1)}{2(G+1)} \tag{21}$$

For $v_0 = 0$, the frequency is progressively down-shifted as the conducting wall is moved further from the plasma. As the distance to the wall tends to infinity, $G \to 1$ and $\omega \to 0$, the marginal condition. For intermediate positions of the conducting wall, the kink mode will have a phase velocity along the magnetic field which is significantly smaller than the Alfvén speed. For example, when $a/b = 0.25$, and using Eq (21), the phase velocity is $\omega/\mid k \mid \simeq 0.09c_A$. Clearly, the phase velocity can be reduced to zero at the marginal condition. This property has already been noted in another context[19].

Returning to Eq (21) with the plasma flow velocity v_0 included, the kink mode solutions can be written

$$\omega = kv_0 \pm \frac{2}{a}\frac{B_{0\theta}^v}{(\rho_0\mu_0)^{1/2}}\left[\frac{(G-1)}{2(G+1)}\right]^{1/2} \tag{22}$$

where the solutions of Eq (23) describe stable kink modes propagating parallel or anti-parallel to the magnetic field. However, when the flow speed exceeds the phase velocity of the kink mode one of the kink modes becomes a negative energy wave, namely the one whose frequency passes through zero. It will be found that this will have important consequences for resistive wall modes, especially as rather low velocities can cause the change in sign of the wave energy when the kink mode is close to the marginal condition.

The effect of a plasma flow velocity on resistive wall modes can now be discussed by returning to the general dispersion relation given in Eq (18). The same approximations are made as in the previous case, namely, the incompressible limit, $c_S \to \infty$, and the long wavelength conditions, $ka \ll 1$, $kb \ll 1$. However, a resistive wall is now assumed instead of a perfect conductor. Hence, finite values of c_W are now included. Under these conditions, Eq (18) can be reduced to

$$\bar{\omega}^2 = k^2 c_A^2 + \frac{(kB_{0Z}^v + \frac{m}{a}B_{0\theta}^v)^2}{\rho_0\mu_0}\frac{G\,(1 + 2imkc_W/(\omega kb(1+(a/b)^{2m})))}{(1 + 2imkc_W/(\omega kb(1-(a/b)^{2m})))} - \frac{(B_{0\theta}^v(a))^2\,m}{\rho_0\mu_0 a^2} \qquad (23)$$

The dispersion relation given in Eq (23) is identical to the one obtained recently by Veeresha et al[15] although these authors wrote the equation in a different form. It is helpful to re-write Eq (23) as follows

$$\omega\left\{\bar{\omega}^2 - k^2c_A^2 - \frac{\left(kB_{0Z}^v + \frac{m}{a}B_{0\theta}^v\right)^2 G}{\rho_0\mu_0} + \frac{(B_{0\theta}^v(a))^2}{\rho_0\mu_0}\frac{m}{a^2}\right\}$$
$$= -\frac{i2mc_W}{b\left[1-\left(\frac{a}{b}\right)^{2m}\right]}\left\{\bar{\omega}^2 - k^2c_A^2 - \frac{\left(kB_{0Z}^v + \frac{m}{a}B_{0\theta}^v\right)^2}{\rho_0\mu_0} + \frac{(B_{0\theta}^v(a))^2 m}{\rho_0\mu_0 a^2}\right\} \qquad (24)$$

Introducing the notation

$$\omega_0^2 \equiv k^2c_A^2 + \frac{\left(kB_{0Z}^v + \frac{m}{a}B_{0\theta}^v\right)^2 G}{\rho_0\mu_0} - \frac{(B_{0\theta}^v(a))^2 m}{\rho_0\mu_0 a^2} \quad , \qquad (25)$$

$$\omega_1^2 \equiv k^2c_A^2 + \frac{\left(kB_{0Z}^v + \frac{m}{a}B_{0\theta}^v\right)^2}{\rho_0\mu_0} - \frac{(B_{0\theta}^v(a))^2\,m}{\rho_0\mu_0 a^2} \quad , \qquad (26)$$

the dispersion relation given in Eq (24) can now be written in the compact form

$$\omega(\bar{\omega}^2 - \omega_0^2) = -\frac{i2mc_W}{b\left[1-\left(\frac{a}{b}\right)^{2m}\right]}(\bar{\omega}^2 - \omega_1^2) \quad . \qquad (27)$$

The meaning of the quantities ω_0 and ω_1 is that $\bar{\omega}^2 = \omega_0^2$ is the dispersion relation for kink modes with a perfectly conducting wall at $r = b$ and $\bar{\omega}^2 = \omega_1^2$ is the corresponding dispersion relation in the absence of a wall. The dispersion relation, Eq (27), is in exactly the same form as the one given by Eq (3a) of Finn and Gerwin[10] for a different equilibrium. It is also worth noting that Eq (27) has the same structure as the dispersion relation derived by Wesson[13].

The dispersion relation given in Eq (27) is the basis of the discussion which follows on resistive wall instabilities and their dependence on a plasma flow velocity. Since the kink

mode dispersion relation with a perfectly conducting wall at $r = b$ contains the three cases of interest, unstable, marginally stable and stable, Eq (27) is used to consider the various cases which might arise. Before continuing with the discussion of resistive wall modes, it should be emphasised that this discussion is of a heuristic nature. Although the dispersion relation given in Eq (27) is treated as being representative of the resistive wall instability, there is always a band of k-values for which the $m = 1$ ideal kink is unstable. The justification for the model is that it allows a comprehensive treatment of the problem to be given and enables further understanding of the underlying mechanisms to be gained. It is hoped that the information obtained from this simple model will serve as a guide for the analysis of more realistic situations and be of some qualitative help to experiment.

It is useful to begin with the case without a flow velocity. The classical resistive wall mode is readily obtained from Eq (27). For this case the plasma is unstable to the ideal kink mode in the absence of a wall, ie $\omega_1^2 < 0$ or $\omega_1^2 = -\gamma_1^2$. In the presence of a perfectly conducting wall at $r = b$, the ideal kink mode is stable, so that $\omega_0^2 > 0$. The dispersion relation, Eq (27) is now written as

$$\omega = -\frac{i2mc_W(\omega^2 + \gamma_1^2)}{b\left[1 - \left(\frac{a}{b}\right)^{2m}\right](\omega^2 - \omega_0^2)} \tag{28}$$

Treating c_W as a perturbation, Eq (28) is solved for the wall mode which is approximated as a zero frequency mode. The correction, $\delta\omega$, to the wall mode frequency, due to a weakly resistive wall, can be obtained perturbatively from Eq (28) by substituting $\omega = 0$ on the right hand side, giving

$$\delta\omega \simeq \frac{i\Gamma\gamma_1^2}{\omega_0^2} \tag{29}$$

where

$$\Gamma \equiv \frac{2mc_W}{b\left[1 - \left(\frac{a}{b}\right)^{2m}\right]} \tag{30}$$

Hence, the stabilised ideal kink mode is destabilized due to the inclusion of finite resistivity of the wall. The growth rate is inversely proportional to the wall time. This is the definition of the MHD resistive wall instability. If $\omega_0^2 < 0$ then the plasma is unstable to an ideal kink with a perfectly conducting wall and the addition of a resistive wall is not significant. It will therefore be assumed that $\omega_0^2 > 0$. Note, also, that if the kink mode is stable without a wall, so that $\omega_1^2 > 0$, then the wall mode solution is

$$\delta\omega \simeq \frac{-i\Gamma\omega_1^2}{\omega_0^2} \tag{31}$$

In this case, the wall mode is damped.

Next, the effect of a plasma flow velocity is considered. Again choosing the condition that $\omega_1^2 = -\gamma_1^2$ it cannot be assumed that the wall mode will still be a zero frequency mode.

Therefore, substituting $\omega = \omega_r + i\gamma$ into Eq (27) and assuming small ω_r

$$\omega_r \simeq \frac{2\gamma k v_0(\gamma + \Gamma)}{(\omega_0^2 - k^2 v_0^2)} \tag{32}$$

$$\gamma \simeq \frac{\Gamma(k^2 v_0^2 + \gamma_1^2)}{(\omega_0^2 - k^2 v_0^2)} \tag{33}$$

Assuming that Γ is small, $\omega_r \ll \gamma$. As before, the wall mode is unstable due to a weakly resistive wall. Since $\omega_r \ll \gamma$, the growth rate can be obtained by perturbing the wall mode about zero frequency as in the case without a flow velocity. Thus, in the presence of a flow velocity, Eq (28) becomes

$$\omega = -\frac{i\Gamma(\bar{\omega}^2 + \gamma_1^2)}{(\bar{\omega}^2 - \omega_0^2)} \tag{34}$$

Perturbing about zero frequency, the correction, $\delta\omega$, to the wall mode frequency is

$$\delta\omega \simeq \frac{i\Gamma(k^2 v_0^2 + \gamma_1^2)}{(\omega_0^2 - k^2 v_0^2)} \tag{35}$$

which is in agreement with Eq (33).

It will be noticed that Eqs (33) and (35) have a pole $\omega_0 = kv_0$. The meaning of this is as follows. When $kv_0 = \omega_0$ one of the kink modes passes through zero frequency and its energy changes sign. When the wall mode and kink mode both have frequencies close to zero they are able to couple. This effect has also been discussed in Refs 10 and 14. The dispersion relation can still be solved perturbatively, as follows.

Assuming the condition

$$kv_0 = \omega_0 \tag{36}$$

the dispersion relation can be written

$$\omega(\omega - kv_0 - \omega_0)(\omega - kv_0 + \omega_0) = -i\Gamma(\bar{\omega}^2 + \gamma_1^2) \tag{37}$$

Perturbing about zero frequency, Eq (37) becomes

$$\delta\omega \cdot (-2\omega_0) \cdot \delta\omega \simeq -i\Gamma(k^2 v_0^2 + \gamma_1^2) \tag{38}$$

Hence

$$(\delta\omega)^2 \simeq i\Gamma\frac{(k^2 v_0^2 + \gamma_1^2)}{2\omega_0} \tag{39}$$

The perturbed frequency is given by

$$\delta\omega \simeq \pm\left[\frac{\Gamma(k^2 v_0^2 + \gamma_1^2)}{4\omega_0}\right]^{\frac{1}{2}}(1+i) \tag{40}$$

The growth rate of the resistive wall mode is therefore enhanced by the coupling to the negative energy kink mode. The growth rate now varies inversely as the square root of the wall time, ie $(c_W/b)^{\frac{1}{2}}$. It is also worth noting that the frequency of the wall mode is comparable to the growth rate under these conditions.

For still higher flow velocities, $kv_0 > \omega_0$, it is the slow kink mode (negative energy) which is destabilized by the resistive wall in a manner analogous to the resistive wall amplifier of Birdsall et al[20]. In this case, the perturbation solution of Eq (37) is obtained by assuming

$$\omega = kv_0 - \omega_0 + \delta\omega \tag{41}$$

Substituting Eq (41) into Eq (37) gives

$$\delta\omega \simeq \frac{i\Gamma(\omega_0^2 + \gamma_1^2)}{2\omega_0(kv_0 - \omega_0)} \tag{42}$$

In this case the frequency of the resistive wall instability is $kv_0 - \omega_0$ and the growth rate is again inversely proportional to the resistive wall time.

The final case to consider is when the plasma is stable to the ideal kink mode in the absence of a wall, ie $\omega_1^2 > 0$. Without a plasma flow velocity, the wall mode is damped by a resistive wall. Now consider the effect of a plasma flow velocity. It can again be shown that $\omega_r \ll \gamma$ for the wall mode so that wall mode stability can still be analysed by perturbing about zero frequency. In this case, the correction to the wall mode frequency can be obtained from Eq (27) and is given by

$$\delta\omega \simeq \frac{i\Gamma(kv_0 - \omega_1)(kv_0 + \omega_1)}{(\omega_0^2 - k^2v_0^2)} \tag{43}$$

It can be seen, that even for this case, the wall mode can become unstable when $v_0 > (\omega_1/k)$. At the threshold $v_0 = (\omega_1/k)$, the real part of the frequency is zero.

As the velocity increases, the growth rate increases. As v_0 approaches (ω_0/k) the wall mode will couple to the negative energy kink mode, again producing a strong enhancement of the growth rate. The resistive wall mode behaves rather like an ideal mode in this case since the higher growth rate $\sim (c_W/b)^{\frac{1}{2}}$ results from a coupling of two modes. A similar interpretation has been given by Finn and Gerwin[9], although these authors refer to the coupling between the wall mode and a backward MHD mode. In fact, as demonstrated above, the coupling occurs when the backward kink mode changes to a forward wave as the frequency passes through zero and the wave energy changes sign. A similar quadratic perturbation analysis for $\delta\omega$ of the dispersion relation, Eq (27), yields

$$\delta\omega \simeq \pm\left[\frac{\Gamma(k^2v_0^2 - \omega_1^2)}{4\omega_0}\right]^{\frac{1}{2}}(1+i) \tag{44}$$

For still higher flow speeds, $v_0 > (\omega_0/k)$, the growth rate falls with increasing v_0 and the corresponding result to Eqs (41) and (42) is

$$\delta\omega \simeq \frac{i\Gamma(\omega_0^2 - \omega_1^2)}{2\omega_0(kv_0 - \omega_0)} \tag{45}$$

The instability again corresponds to the slow kink mode with a frequency $\omega = kv_0 - \omega_0$.

V SUMMARY AND CONCLUSIONS

Experimental results[3] from the DIII-D tokamak have suggested that, in the presence of toroidal rotation the lifetime of the discharge can be significantly extended. This has provided the motivation for the present attempt to gain some insight into the role of a plasma flow velocity on the resistive wall instability and whether there are any critical flow velocities. For this purpose a simple, sharp boundary cylindrical model with a skin current, axial flow and a thin resistive wall has been studied.

The classic resistive wall instability results from an external kink mode which is unstable without a wall but is stabilized by the presence of a perfectly conducting wall. When the finite resistivity of the conducting wall is included the system is unstable to the resistive wall mode, growing on the slower time scale of the resistive wall. These are the essential features of the resistive wall instability and are all contained in the present model. However, it should be remembered that the results obtained from this model can only be used as a qualitative guide to the behaviour of resistive wall modes. This is because the sharp boundary, surface current model is always unstable to an $m = 1$, ideal kink mode.

Although this model is oversimplified, it allows the physical mechanisms to be more easily identified. These mechanisms would be expected to play a role in more realistic models. This expectation is supported by the work of Finn and Gerwin[10] who have also examined a cylindrical model but one in which an equilibrium current flows in the plasma. The dispersion relation obtained in Ref 10 has the same form as the one derived in this paper. The analytic results given in the present paper are complementary to the numerical results obtained in Ref 10.

The effect of a flow velocity was first considered for the ideal kink mode with a perfectly conducting wall. In particular, the properties of wall stabilized kink modes have been discussed. Far from marginal stability the phase velocity of kink modes along the magnetic field is of the order of the Alfvén speed. However, these modes are down-shifted in frequency as the condition of marginal stability for the ideal kink mode is approached with the result that the parallel phase speed can become much smaller than the Alfvén speed, tending to zero at the marginal condition.

In the presence of a parallel flow velocity, the kink modes are Doppler shifted in frequency so that the waves propagating parallel and anti-parallel to the magnetic field have frequencies $\omega = kv_0 \pm \omega_0$, where ω_0 is the frequency of the mode without flow. It is noted that the mode

$\omega = kv_0 - \omega_0$ passes through zero frequency when $v_0 = \omega_0/k$ and that the change in sign of the frequency corresponds to a change in sign of the wave energy. This is an MHD example of a wave carrying negative energy when the flow speed exceeds the phase speed of the wave in the medium[21]. Under these conditions the two waves, $\omega = kv_0 \pm \omega_0$ are often referred to as fast and slow waves.

Resistive wall modes are discussed making use of this point of view. These modes are only of significance when the ideal kink modes can be stabilised by a perfectly conducting wall. It is clear that any rotation can destabilize a resistive wall mode depending on the proximity of the marginal condition for a perfectly conducting wall. If a plasma without a parallel flow velocity is stable in the absence of a wall then it remains so if a resistive wall is introduced. However, in the presence of a flow velocity, a resistive wall instability can occur when $v_0 > \omega_1/k$ where ω_1 is the kink mode frequency without a wall. When the plasma is unstable without a wall, $\omega_1^2 < 0$, but stabilized by a perfectly conducting wall, the resistive wall instability is further destabilized at a critical flow speed, $v_0 = \omega_0/k$, when the zero frequency, negative energy kink mode couples to the zero frequency wall mode. Under these conditions the resistive wall instability behaves more like an ideal instability and the growth rate is proportional to $(c_W/b)^{\frac{1}{2}}$, ie to the inverse of the square root of the wall time.

For still larger values of $v_0 > (\omega_0/k)$ it is the negative energy kink mode, rather than the wall mode, with a frequency $kv_0 - \omega_0$, which is unstable in the presence of a resistive wall, in a manner reminiscent of the resistive wall amplifer[20]. In this case, the growth rate is again inversely proportional to the wall time (c_W/b) and varies inversely with the flow speed v_0. Hence, although all flow speeds are evidently destabilizing, a system driven at a higher flow velocity, ie $v_0 > (\omega_0/k)$, will be subject to a weaker instability than for the smaller flow speed, $v_0 \simeq (\omega_0/k)$.

The final conclusion is that there are two critical velocities. The first, $v_0 = (\omega_0/k)$, is the more threatening since at this velocity, the resistive wall instability would have a growth rate closer to an ideal instability. The other critical velocity is $v_0 = (\omega_1/k)$, corresponding to the case when the plasma is stable in the absence of a wall. When this velocity is exceeded, the plasma is again unstable to a resistive wall instability. Since $\omega_1 < \omega_0$, this instability is also enhanced when $v_0 = (\omega_0/k)$ and becomes weaker as v_0 increases further as discussed for the case where $\omega_1^2 < 0$. If (ω_0/k) is low, ie the plasma is close to marginal stability, a velocity $v_0 \gg (\omega_0/k)$ would be preferred whereas if the plasma is not near the marginal condition, $v_0 < (\omega_0/k)$ might be preferable. In either case, the plasma would only be subjected to a weak instability rather than the strong instability associated with the critical velocity, $v_0 = (\omega_0/k)$.

ACKNOWLEDGEMENTS

I would like to thank Chris Gimblett and John Wesson for helpful discussions and Mikhail Gryaznevich for his encouragement. This work was funded jointly by the UK Department of Trade and Industry and EURATOM.

REFERENCES

[1] D Pfirsch and H Tasso, *Nucl Fusion* **11**, 259 (1971).

[2] A M Garofalo, A D Turnbull, E J Strait et al, *Physics of Plasmas*, **6**, 1893 (1999).

[3] J Luxon, P Anderson, F Batty et al, *Plasma Physics and Controlled Nuclear Fusion Research*, 1986 [International Atomic Energy Agency, Vienna 1987] Vol I p159.

[4] C G Gimblett, *Nuclear Fusion* **26**, 617 (1986).

[5] C G Gimblett, *Plasma Phys Contr Fus* **31**, 2183 (1989).

[6] A Bondeson and D Ward, *Phys Rev Lett* **72**, 2709 (1994).

[7] R Betti and J P Freidberg, *Phys Rev Lett* **74**, 2949 (1995).

[8] J M Finn, *Phys Plasmas* **2**, 198 (1995).

[9] R Fitzpatrick and A Aydemir, *Nuclear Fusion* **36**, 2344 (1996).

[10] J M Finn and R A Gerwin, *Phys Plasmas* **3**, 2344 (1996).

[11] M S Chu, J M Greene, T H Jensen, R L Miller, A Bondeson, R W Johnson and M E Maul, *Phys Plasmas* **2**, 2236 (1995).

[12] C G Gimblett and R J Hastie, *Phys Plasmas* **7**, 258 (2000).

[13] J A Wesson, *Phys Plasmas* **5**, 3816 (1998).

[14] C N Lashmore-Davies, J A Wesson and C G Gimblett, *Phys Plasmas* **6**, 3990 (1999).

[15] B M Veeresha, S N Bhattacharyya and K Avinash, *Phys Plasmas* **6**, 4479 (1999).

[16] V D Shafranov, J Nucl Energy II, **5**, 86 (1957).

[17] R J Tayler, *Proc Phys Soc* **B70**, 1049 (1957).

[18] W M Manheimer and C N Lashmore-Davies, MHD and Microinstabilities in Confined Plasma (Adam Hilger, Bristol, 1989) p49-52.

[19] H Bindslev and C N Lashmore-Davies, 26th EPS Conference on Controlled Fusion and Plasma Physics, Maastricht 1999.

[20] C K Birdsall, G R Brewer and A V Haeff, Proc IRE **41**, 865 (1953).

[21] P A Sturrock, *J Appl Phys* **31**, 2052 (1960).